Comparison of the Calibration of Ionospheric Delay in VLBI Data by the Methods of Dual Frequency and Faraday Rotation

J. A. Scheid
Tracking Systems and Applications Section

When both S-band and X-band data are recorded for a signal which has passed through the ionosphere, it is possible to calculate the ionospheric contribution to signal delay. In Very Long Baseline Interferometry (VLBI) this method is used to calibrate the ionosphere. In the absence of dual frequency data, the ionospheric content measured by Faraday rotation, using a signal from a geostationary satellite, is mapped to the VLBI observing direction. The purpose of this article is to compare the ionospheric delay obtained by these two methods. The principal conclusions are: 1) the correlation between delays obtained by these two methods is weak; 2) in mapping Faraday rotation measurements to the VLBI observing direction, a simple mapping algorithm which accounts only for changes in hour angle and elevation angle is better than a more elaborate algorithm which includes solar and geomagnetic effects; 3) fluctuations in the difference in total electron content as seen by two antennas defining a baseline limit the application of Faraday rotation data to VLBI.

I. Introduction

In VLBI, two or more antennas track the same extragalactic source simultaneously, and at each station the received signal is digitized and recorded on magnetic tape. The tapes from a pair of stations are then correlated to determine the time delay between the arrival of a wave front at one station and the arrival of the same wave front at the other. The total delay has geometric, tropospheric, ionospheric and instrumental components,

$$\tau = \tau_G + \tau_T + \tau_{Ib} + \tau_{Cb}, \qquad b = S, X \tag{1}$$

The geometric delay τ_G is nondispersive. For the purposes of this analysis, tropospheric delay τ_T is considered nondispersive. Ionospheric delay τ_I is dispersive. Instrumental delay τ_C includes the station clock offsets as well as dispersive components due to differences in the antennas and electronics at the two stations. Accordingly, the ionospheric and instrumental delays carry the subscript b to indicate the frequency band of the observation.

The excess phase delay due to the propagation of radiation through a dispersive medium is given for a single frequency by

$$\tau = \frac{1}{c}\int dS\,(n - 1) \tag{2}$$

where n is the index of refraction, c is the velocity of light in vacuum and the integration is over the ray path (see Ref. 1 for

basic ionospheric formulas). The major effect of the ionosphere is due to a plasma of free electrons. Under the assumption that damping due to electron collisions is negligible, the index of refraction at a point in the ionosphere is given by

$$n = (1 - r)^{1/2}$$
$$r = \frac{f_P^2}{f_b^2 + f_b f_H \cos\phi} \tag{3}$$

where f_b is the observing frequency in band b, f_P is the plasma frequency, f_H is the frequency of precession of an electron in the geomagnetic field, and ϕ is the angle between the wave normal and the direction of the magnetic field. Plasma frequency in Hertz is related to electron density d in electrons per cubic meter by

$$f_P = 8.984\, d^{1/2} \tag{4}$$

Expanding the expression for n, the quantity $n - 1$ to be integrated along the ray path takes the form

$$n - 1 = -\frac{1}{2} r - \frac{1}{8} r^2 \ldots \tag{5}$$

Normally for the plasma of the ionosphere, $f_H < f_P < 15$ MHz. For frequencies of interest in VLBI experiments, $f_P << f_b$. Consequently, a first order approximation to $n - 1$ is obtained by neglecting the geomagnetic field and retaining only the terms quadratic in r,

$$n - 1 = -\frac{1}{2} \frac{f_P^2}{f_b^2} \tag{6}$$

In this approximation, the group delay at a single station caused by the ionosphere is given by

$$\frac{40.31}{c f_b^2} \int dh \frac{D(h)}{\cos\alpha} \tag{7}$$

where h is elevation in meters, $D(h)$ is the electron density profile in electrons per cubic meters, and α is the angle between the local vertical and the tangent to the ray to the source. Neglecting the bending of the ray, Eq. (7) is approximated by

$$\frac{40.31}{c f_b^2} \quad \frac{TEC}{\cos\alpha} \tag{8}$$

where TEC is the columnar total electron content at zenith for station i.

For VLBI observations, the quantity of interest is the difference between the delays at the two stations with respect to a common reference point,

$$\tau_{Ib} = \frac{40.31}{c f_b^2} \left[\frac{TEC_1}{\cos\alpha_1} - \frac{TEC_2}{\cos\alpha_2} \right] \tag{9}$$

II. Dual Frequency Method

In reference to Eq. (9), the total observed delay may be approximated by

$$\tau_b = \tau_o + \frac{N}{f_b^2} \tag{10}$$

Thus a measurement of the delay at two frequencies makes possible the determination of the constants τ_o and N so that τ_b may be removed from the total delay at both frequencies.

In processing VLBI data, the ionospheric contribution to delay is determined in the program CALIBRATE for both the dual frequency and Faraday rotation methods. The frequencies used in CALIBRATE are weighted averages of the channel frequencies in each band. In the dual frequency approach, the quantities

$$A = \frac{(f_S^2 \tau_S - f_X^2 \tau_X)}{(f_S^2 - f_X^2)}$$
$$B = f_S^2 f_X^2 \frac{(\tau_X - \tau_S)}{(f_S^2 - f_X^2)} \tag{11}$$

are computed (Ref. 2). If Eq. (10) were exact, the quantities A and B would equal τ_o and N respectively. Contributions to dispersion other than those of Eq. (10), however, introduce frequency dependent terms into A and B. Such contributions are present but are known or assumed to be constant in time. Terms known to be small were omitted by truncating the expansion of the index of refraction and neglecting the geomagnetic field.

The data processed by CALIBRATE have been corrected by phase calibration to remove instrumental effects. The component of instrumental phase shift which is independent of frequency appears in the delay observable as a term proportional to $1/f$. If this is not eliminated by phase calibration, it will contaminate the determination of both τ_o and N. Any instrumental delay inversely proportional to frequency squared which is not removed by phase calibration contributes directly to the value of N determined from the data.

III. Faraday Rotation Method

Faraday rotation refers to the rotation of the axis of the polarization ellipse of an electromagnetic wave as it propagates through a magnetized plasma. The total Faraday rotation in radians due to passage of the wave through the ionosphere in the presence of the geomagnetic field is given by

$$\frac{\pi}{cf^2}\int dh\, f_H\, f_P^2\, \frac{\cos\phi}{\cos\alpha} \tag{12}$$

Faraday rotation is measured along the ray path of a signal from a geostationary Applications Technology Satellite (ATS) to a ground receiving station at Goldstone. Total electron content for this slanted ray path is then computed and mapped to the zenith at the zenith reference point. The zenith reference point is defined to be the point along the ray path between the ATS and the ground station at a reference altitude, typically 350 km. The result, the reference point zenith electron content, is the form of the Faraday rotation data which is input to CALIBRATE.

In CALIBRATE these data are mapped to the ray path through the ionosphere along the lines of sight from the VLBI stations to the source. This mapping is designed to account for several differences between the conditions of the Faraday rotation measurement and those of the VLBI observation (Ref. 3). These include factors to account for changes in hour angle, solar-zenith angle, geomagnetic latitude and elevation angle.

Solar-zenith angle is the angle between the observer's zenith and the sun. The solar-zenith angle dependence of vertical ionospheric electron profile has been modeled by Chapman (Ref. 3) and by Yip, von Roos and Escobal (Ref. 4). Parameters in the SEASAT altimeter semi-empirical model of S. C. Wu (private communication, 1977) applied in this analysis are determined by least-squares fitting to the measured zenith electron content. Daytime zenith electron content is lower during summer than during winter while nighttime zenith electron content remains higher during summer. Thus the model parameters vary during the year.

The geomagnetic adjustment is complicated by a "geomagnetic anomaly." During early morning hours, the concentration of ionospheric electrons is higher at the magnetic equator and lower at the geomagnetic poles. As the ionosphere is illuminated by the sun, electrons drift to the north and south away from the magnetic equator reducing the electron concentration at the magnetic equator by about 10 percent. This time dependence is parameterized in the model of Wu.

The model used to compute ionospheric delay from Faraday rotation data refers to the combination of mapping factors used. In this analysis two models for treating the Faraday rotation data are compared. Model 1 accounts for changes in hour angle, elevation angle, solar zenith angle and geomagnetic latitude. Model 2 accounts for changes in hour angle and elevation only. In either case, the difference in ionospheric delay between VLBI stations is calculated according to Eq. (9) from the mapped total electron content.

IV. Data

The VLBI data used in this analysis are for the 257.6-km baseline between the Owens Valley Radio Observatory (OVRO) near Big Pine, California and Deep Space Station 13 (DSS 13) at the Goldstone Tracking Station near Barstow, California. These data were collected using the Mark III VLBI data acquisition system during Mobile VLBI experiments 81A, 81B and 81C conducted on February 15, 17 and 18 respectively in 1981. Correlation of these experiments was done at the Haystack Observatory, Westford, Massachusetts. Phase calibration was applied in all three experiments. The mean frequencies for the S and X bands were 2289.901 MHz and 8437.9102 MHz, respectively. Typical system error for synthesized delay in these data is 0.05 nanoseconds.

Values of columnar total electron content at intervals of one hour were extracted from Faraday rotation data covering the time period of the VLBI experiments. These data, used in CALIBRATE to interpolate to the mean time of the VLBI observations, are plotted in Fig. 1 in units of 10^{17} electrons per square meter as a function of local time in hours.

For the purpose of comparing the ionospheric delay calculated by the dual frequency and Faraday rotation methods, the delays were averaged over all observations in an experiment and the average was subtracted from the ionospheric delays. Thus, the scatter of the ionospheric delay about the experimental means are the quantities being compared. From Eq. (13), the ratio of ionospheric delay at X-band to that at S-band is roughly 0.08. Thus, S-band ionospheric delays are dominant and they are the data used in this analysis.

In all plots there is one point for each observation. The average time interval between observation mean times is about twenty minutes. A few points in the data had anomalously large delays. Observations resulting in delays outside of the range -3.0 to +3.0 nanoseconds were excluded from the analysis. Figures 2, 3 and 4 present the ionospheric delay scatter obtained from both methods plotted against local time for experiments 81A, 81B and 81C, respectively. In the plots against local time, the experiments proceed from the start time of the experiment to 24 hours on the right and are then continued from 0 hours on the left.

V. Discussion

In Fig. 5, the Faraday rotation data for both mapping models are plotted against the dual frequency data. In these scatter plots the data of the three experiments are combined and plotted in the form of deviations from the mean normalized with the standard deviations. Also shown in each figure are the lines of regression, the slopes of which are the correlation coefficients. Since the data are presented in the form of deviations from the mean, the line of regression passes through the origin. The correlation coefficients are 0.23 and 0.47 for models 1 and 2, respectively. Thus, while there is a positive correlation between the dual frequency and Faraday rotation methods of obtaining ionospheric delay, it is a weak correlation. Furthermore, the correlation is made worse rather than better by the inclusion of mapping factors which incorporate solar zenith angle and geomagnetic latitude effects.

In Fig. 6, the data from the three experiments are superimposed in the same plot against local time. In the three experiments, the Faraday rotation data are seen to track very closely, the dual frequency data less well. The same 24-hour schedule was shifted and used for all three experiments. These experiments were consecutive and were performed within a four-day period so that the same sources were being observed at the same local times during each experiment to within a few minutes. The variation of the Faraday rotation data with time of day was similar for the three experiments, so that the kind of tracking seen in the Faraday rotation data of Fig. 6 is expected.

Ionospheric variations may be classified in three categories: large-scale spacial (>500 km), large-scale temporal (>1 h) and small-scale (<500 km or <1 h) variations (Ref. 5). Large-scale effects are modeled in the mapping of the Faraday rotation data. Thus, to a first approximation the large-scale effects may be removed from the dual frequency data by subtracting from it the Faraday rotation data. This difference, plotted in Fig. 7, should retain only the effect that small-scale ionospheric variations and irregularities produce in the dual frequency data by virtue of the fact that in this method ionospheric delay is measured independently at each station. We see, however, that the data of model 1, in contrast to that of model 2, contain a diurnal signature. This suggests that the model 1 mapping function introduces a large-scale effect into the data.

Based on the Faraday rotation data, day hours were taken to be 0700 to 2100 local time. Standard deviations σ_D and σ_N for the day and night periods, respectively, of the data in Fig. 7 are given in Table 1. Let us assume that there is a component of the fluctuation in the measured ionospheric delay which is proportional to the total electron content. This implies

$$\sigma_{ID} = R\sigma_{IN} \tag{13}$$

where σ_{ID} and σ_{IN} are respectively the day and night standard deviations of the ionospheric delay, and R is the ratio of the average total electron content of day to that of night. In Table 1, the ratio σ_D/σ_N is 1.48 and 1.35 for the data based on mapping models 1 and 2, respectively. From the Faraday rotation data, the average total electron content of the ionosphere, in units of 10^{17} electrons per square meter, was found to be 1.88 and 5.62 for night and day, respectively, so that R = 2.99. The fact that R is different from σ_D/σ_N may be interpreted to indicate that there is an additional component σ_o of the ionospheric delay scatter which is independent of changes due to sunlight. Thus,

$$\begin{aligned} \sigma_D^2 &= \sigma_{ID}^2 + \sigma_o^2 \\ \sigma_N^2 &= \sigma_{IN}^2 + \sigma_o^2 \end{aligned} \tag{14}$$

From Eqs. (13) and (14) one finds the values of σ_{ID}, σ_{IN} and σ_o listed in Table 1.

Two points can be made about the statistics of Table 1. First, that the scatter in the data associated with model 1 is significantly larger than that associated with model 2, reflecting the weaker correlation of the model 1 Faraday rotation data to the dual frequency data. Second, that σ_o, the component of scatter in ionospheric delay which is constant, is comparable in size to σ_{ID}, the component associated with sunlight. System noise error for these data, based on the number of bits correlated, is approximately 0.05 nanoseconds and is therefore too small to account for σ_o. Possibly the component which is independent of total electron content is introduced during data acquisition and processing. On the

other hand, it may be that the assumption of Eq. (13) is incorrect.

Rays from the ends of a baseline in the direction of an extragalactic source penetrate the ionosphere along parallel lines separated by the baseline distance. For the relatively short baseline of these data, fluctuations in ionospheric delay can be estimated according to

$$\sigma_\tau = A(L/10)^{0.75}\tau \qquad (15)$$

where L is the distance in kilometers between points in the ionosphere and A is a dimensionless constant (Ref. 5). Since ionospheric delay is proportional to total electron content, the estimate of the standard deviation given by Eq. (15) is proportional to total electron content and is therefore comparable to the quantities of σ_{ID} and σ_{IN}. Using the average values of total electron content for day and night, the average ionosperic delay is computed from Eq. (8) to be 14.4 and 4.8 nanoseconds, respectively, for day and night observations. From the values of σ_{ID} and σ_{IN} given in Table 1, we find the constant A to be 0.0045 and 0.0027 for models 1 and 2 respectively. Callahan finds values of A in the range 0.0040 to 0.0031. This agreement supports the contention that the delay scatter seen in Fig. 7 is due to small-scale variations in the ionosphere.

VI. Conclusions

The weakness of the correlation between ionospheric delay computed by the dual frequency and Faraday rotation methods supports the conclusion of J. M. Davidson (private communication, 1981), obtained for the ARIES Project, that the ionosphere has not been adequately modeled in the mapping function applied to Faraday rotation data to calibrate VLBI data. Ionospheric delay computed from Faraday rotation data depends on the measurement of total electron content along a single ray path through the ionosphere. Ionospheric delay determined by the dual frequency method depends on the difference between the total electron content along two rays through the ionosphere separated by the baseline distance. The dual frequency method therefore incorporates fluctuations due to differences in the ionosphere along the two rays. Since these fluctuations cannot be modeled, the Faraday rotation method cannot be used to compute the ionospheric delay calibration at the level required for processing VLBI data.

In this analysis, one component of fluctuation in ionospheric delay obtained by the dual frequency method is associated with variations in the total electron content of the ionosphere induced by sunlight. The other component is found to be independent of day-night variations in the ionosphere. System noise error is too small to account for the solar independent component.

Acknowledgments

The Faraday rotation data was supplied by H. N. Royden. The author wishes to thank G. E. Lanyi, G. H. Purcell, J. L. Fanselow and H. N. Royden for helpful discussions.

References

1. Meaks, M. L., *Methods of Experimental Physics,* Vol. 12, part B. New York: Academic Press, 1976.

2. Thomas, J. B., "An Analysis of Radio Interferometry with the Block O System," *JPL Publication 81-49,* Jet Propulsion Laboratory, Pasadena, California, December, 1981.

3. Chapman, S., "The Absorption and Dissociative or Ionizing Effect of Monochromatic Radiation in an Atmosphere on a Rotating Earth," *Proc. Phys. Soc.* (London), Vol. 43, p. 25, 1931.

4. von Roos, O. H., Yip, K. B. W. and Escobal, P. R. "A Global Model of the Earth's Ionosphere for Use in Space Applications," *Astronautica Acta,* Vol. 18 (Supplement), p. 215, Pergamon Press, 1974.

5. Callahan, P. S., "Ionospheric Variations Affecting Altimeter Measurements: A Brief Synopsis," *Marine Geodesy,* Vol. 8, Numbers 1-4, 1984.

Table 1. Statistics for dual frequency delay scatter minus Faraday rotation delay scatter. The day and night data includes 107 and 68 data points, respectively.

	Model 1	Model 2
σ_D	0.936 nsec	0.618 nsec
σ_N	0.631 nsec	0.457 nsec
σ_D/σ_N	1.48	1.35
σ_{ID}	0.733 nsec	0.441 nsec
σ_{IN}	0.244 nsec	0.147 nsec
σ_o	0.592 nsec	0.433 nsec
A	0.0045	0.0027

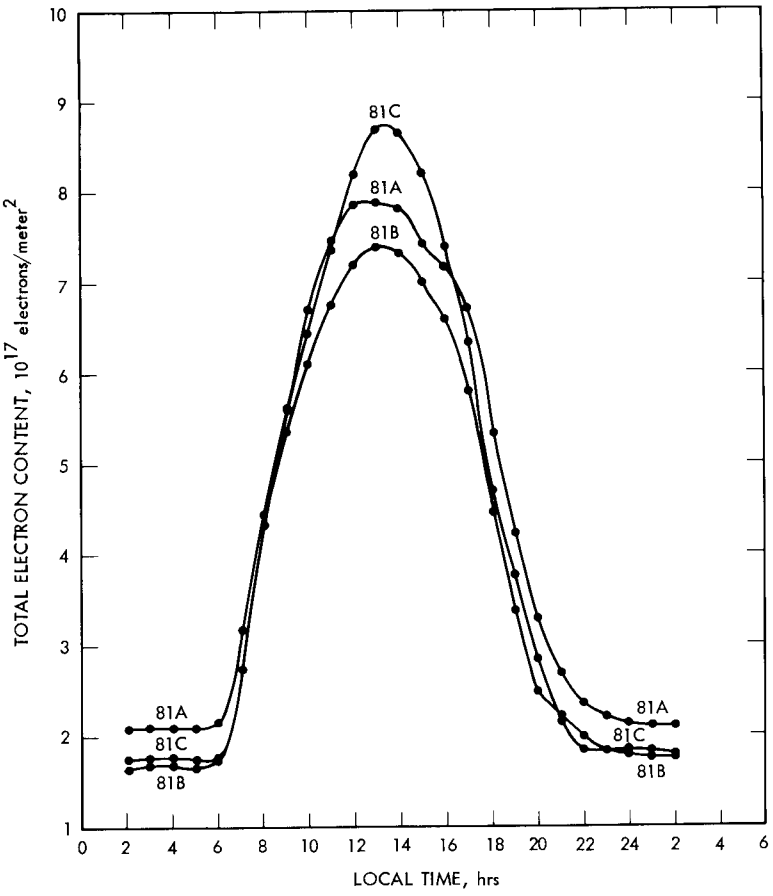

Fig. 1. Columnar total electron content of the ionosphere determined by the Faraday rotation method in units of 10 electrons per square meter versus local time, experiments 81A, 81B and 81C.

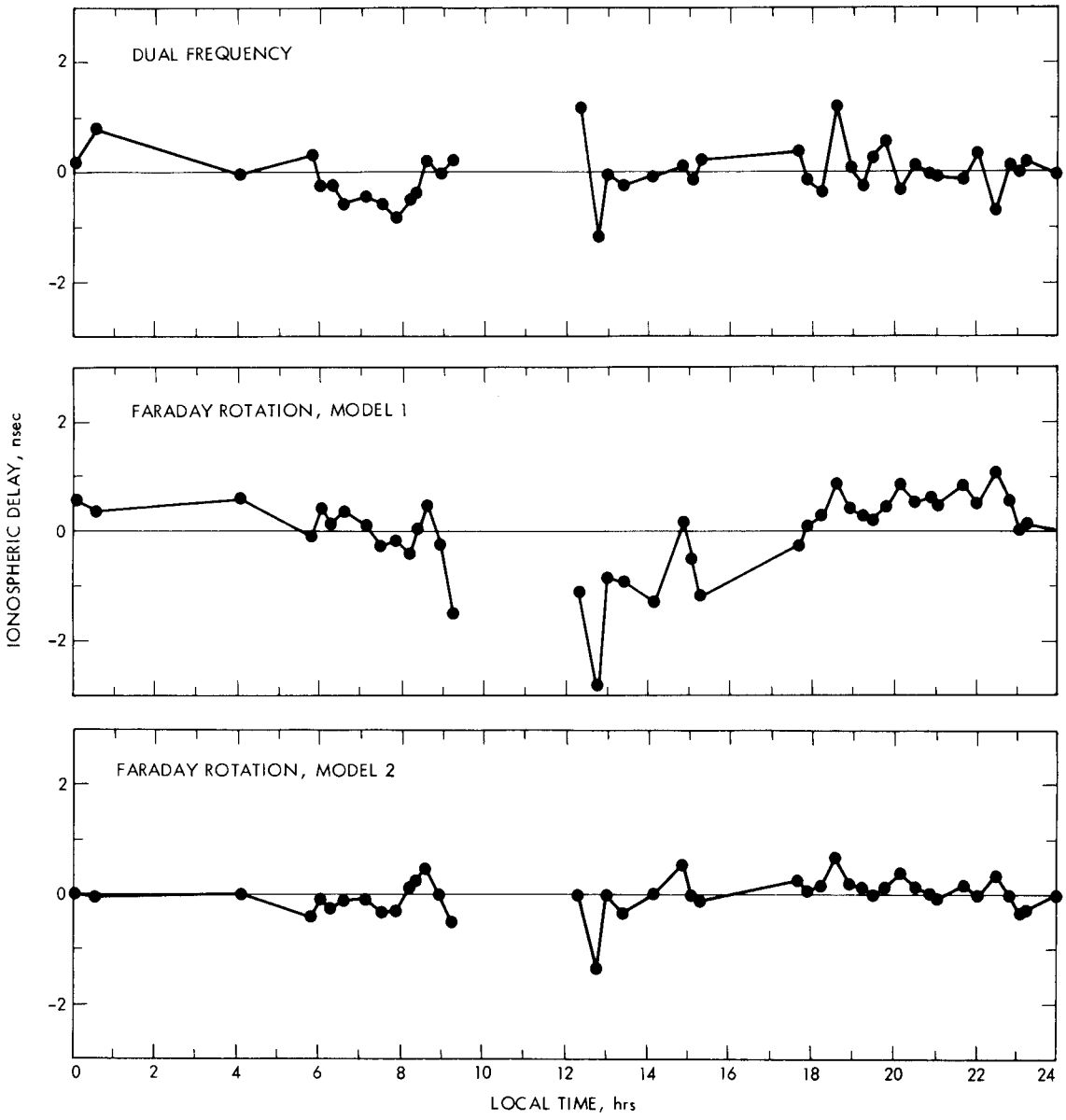

Fig. 2. S-band ionospheric delay scatter versus local time, experiment 81A

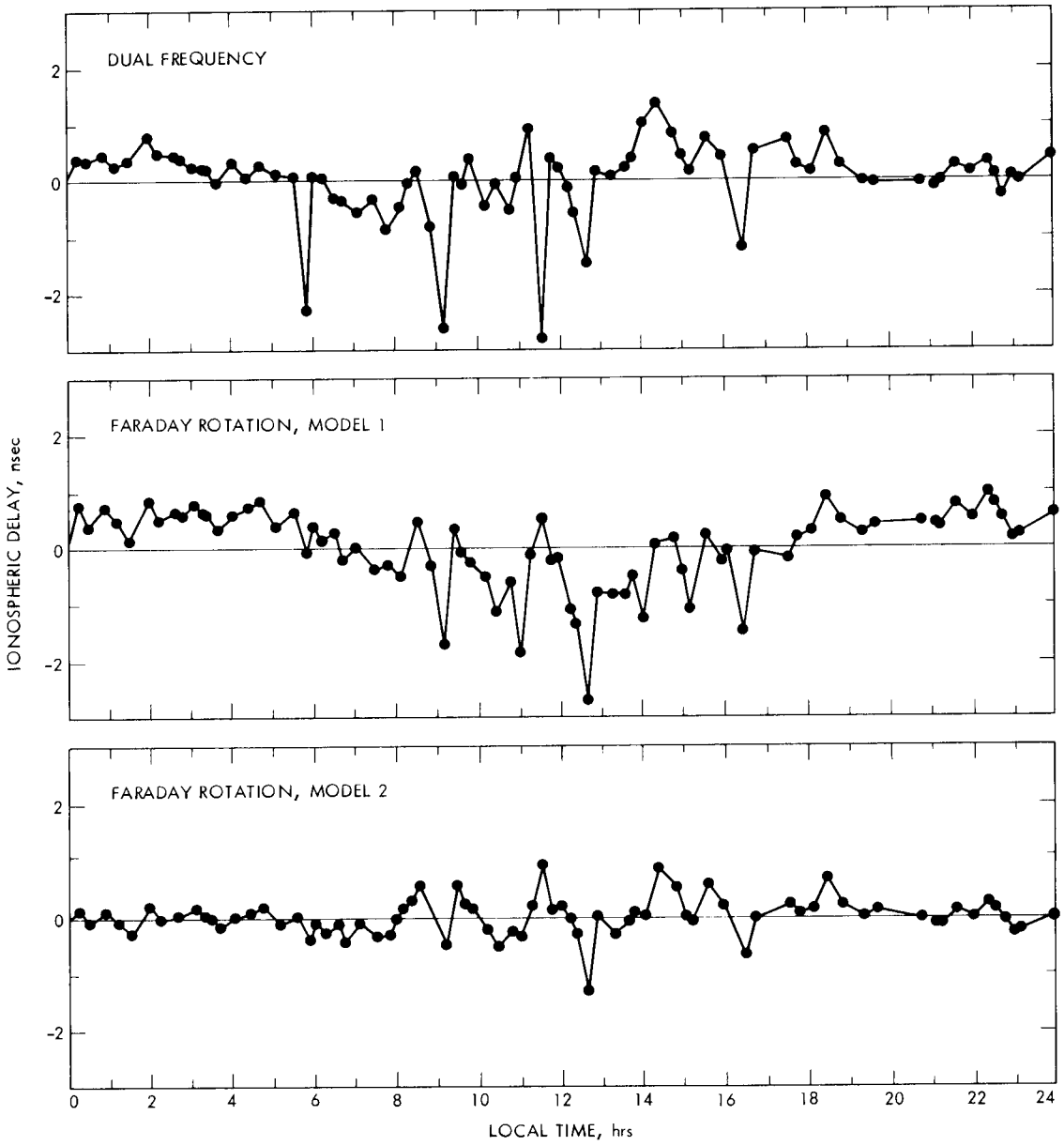

Fig. 3. S-band ionospheric delay scatter versus local time, experiment 81B

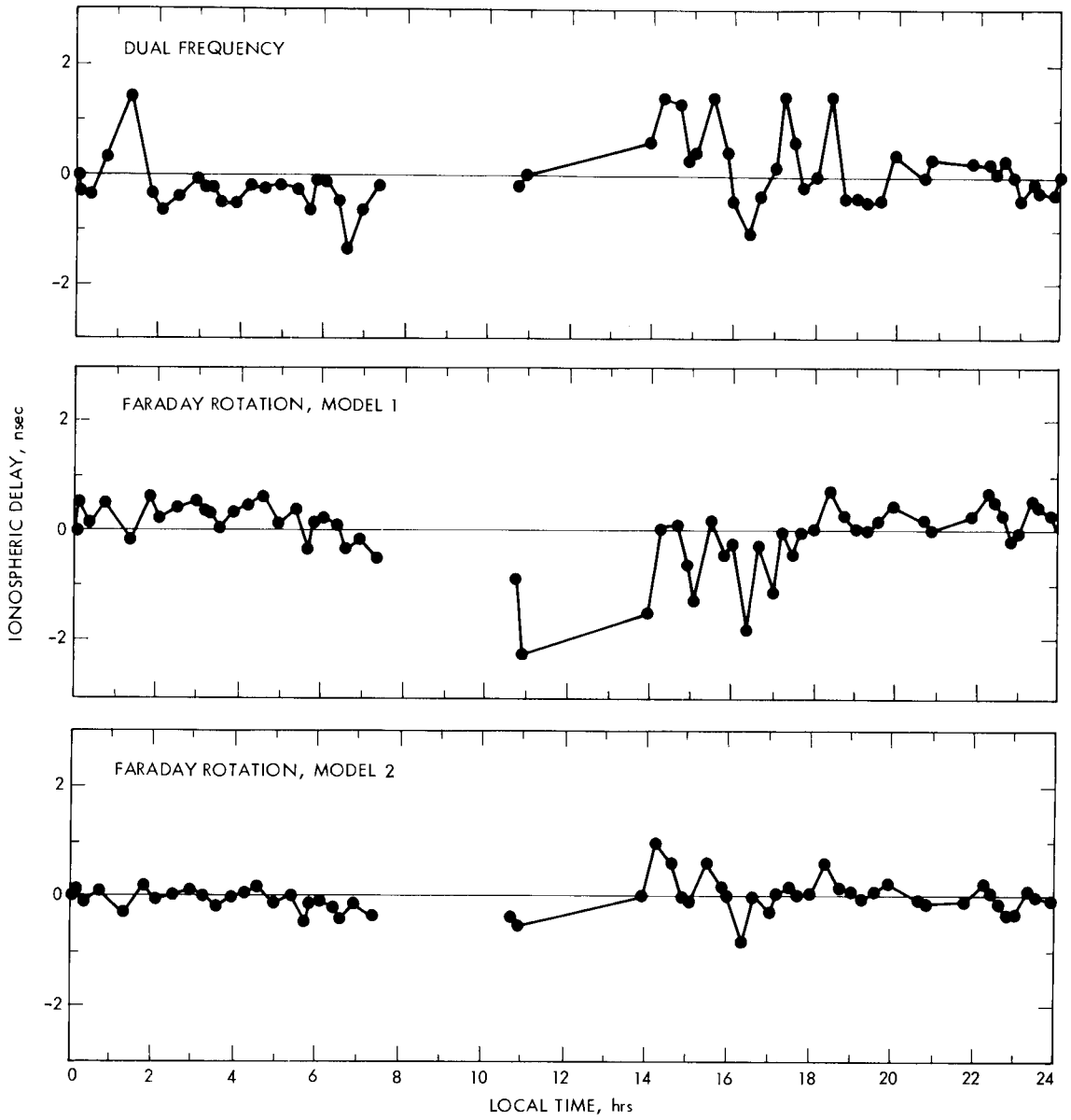

Fig. 4. S-band ionospheric delay scatter versus local time, experiment 81C

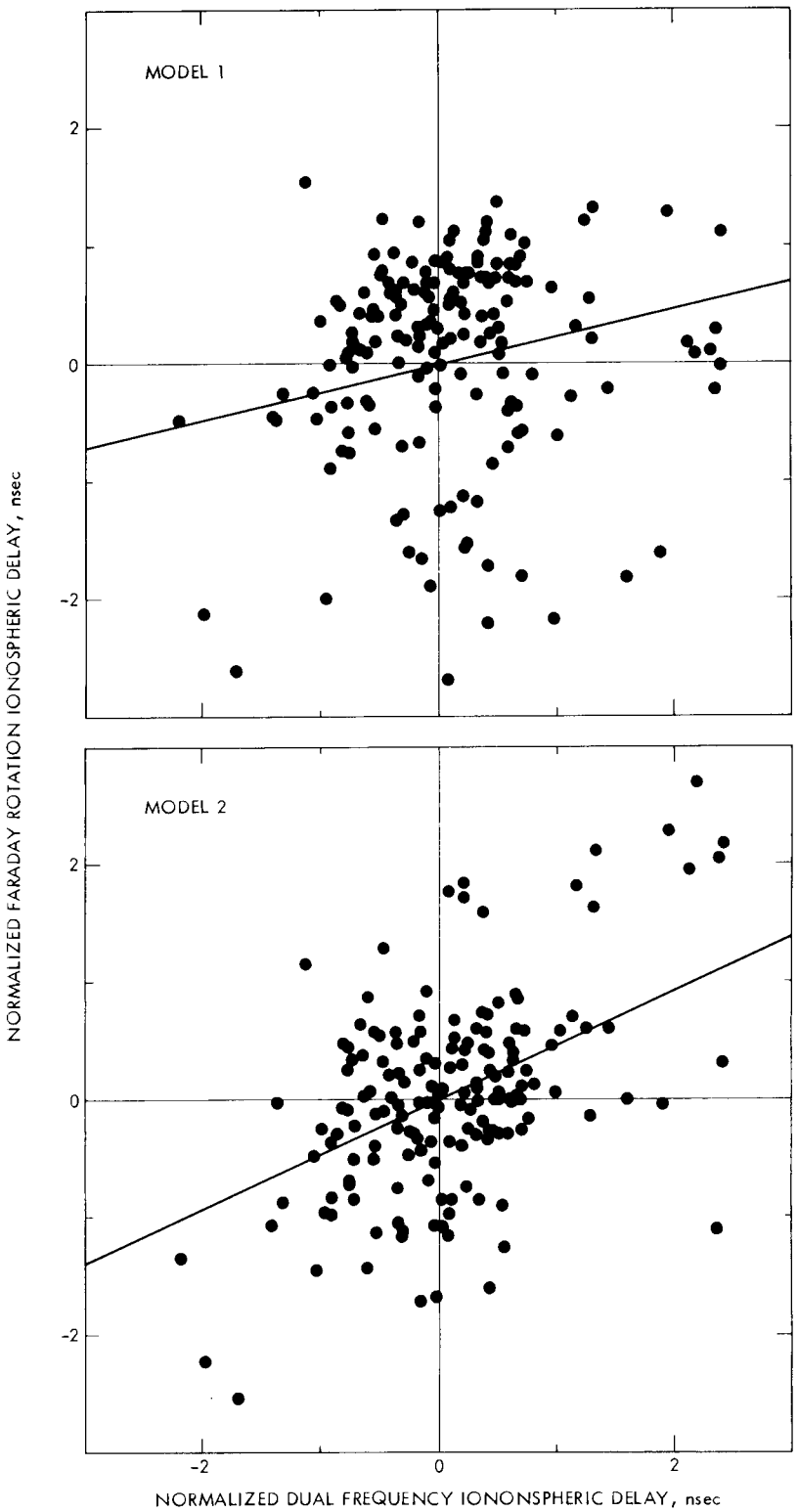

Fig. 5. Dual frequency delay scatter versus Faraday rotation delay scatter at S-band, experiments 81A, 81B and 81C

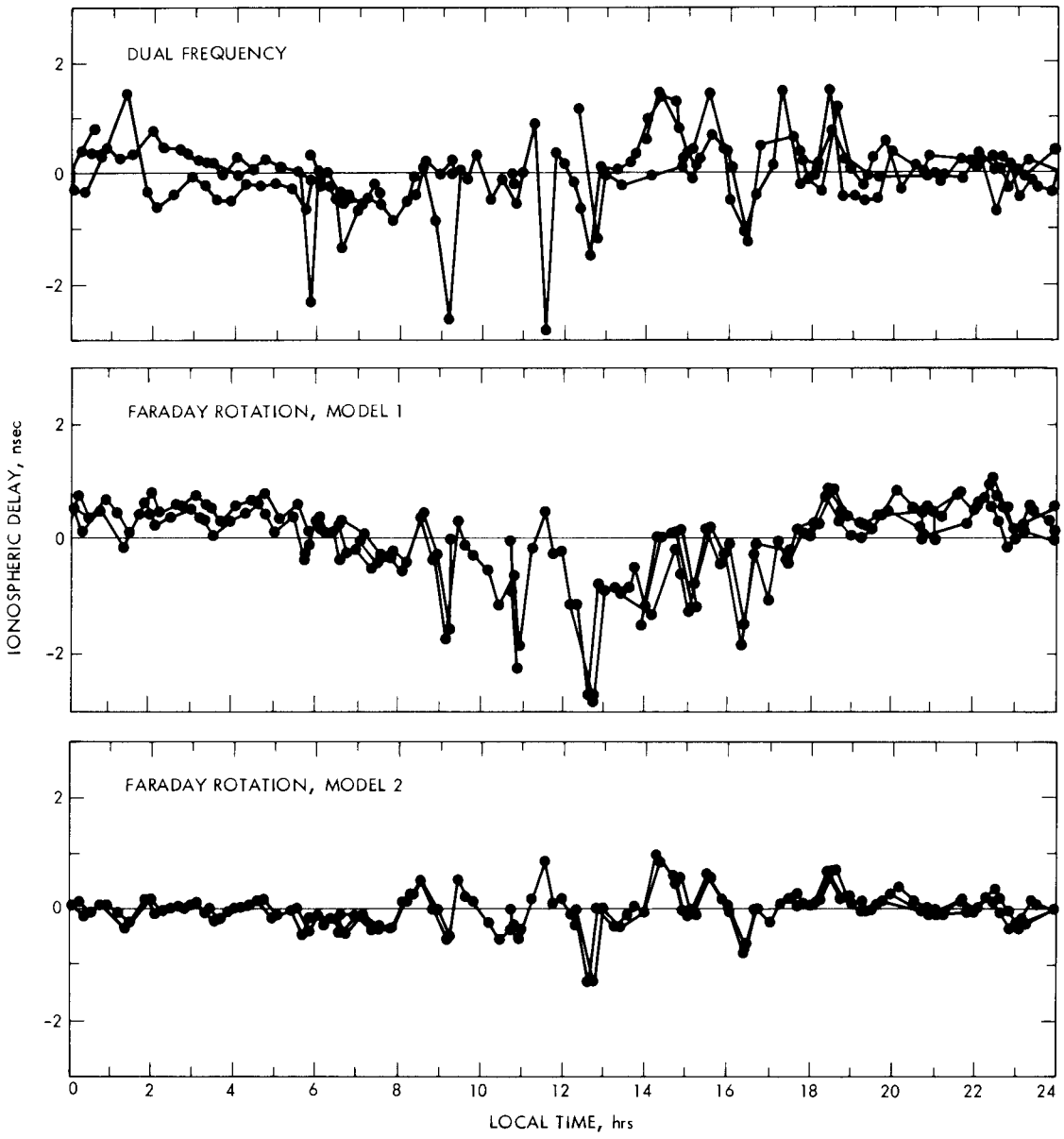

Fig. 6. Dual frequency and Faraday rotation ionospheric delay scatter versus local time at S-band, experiments 81A, 81B and 81C

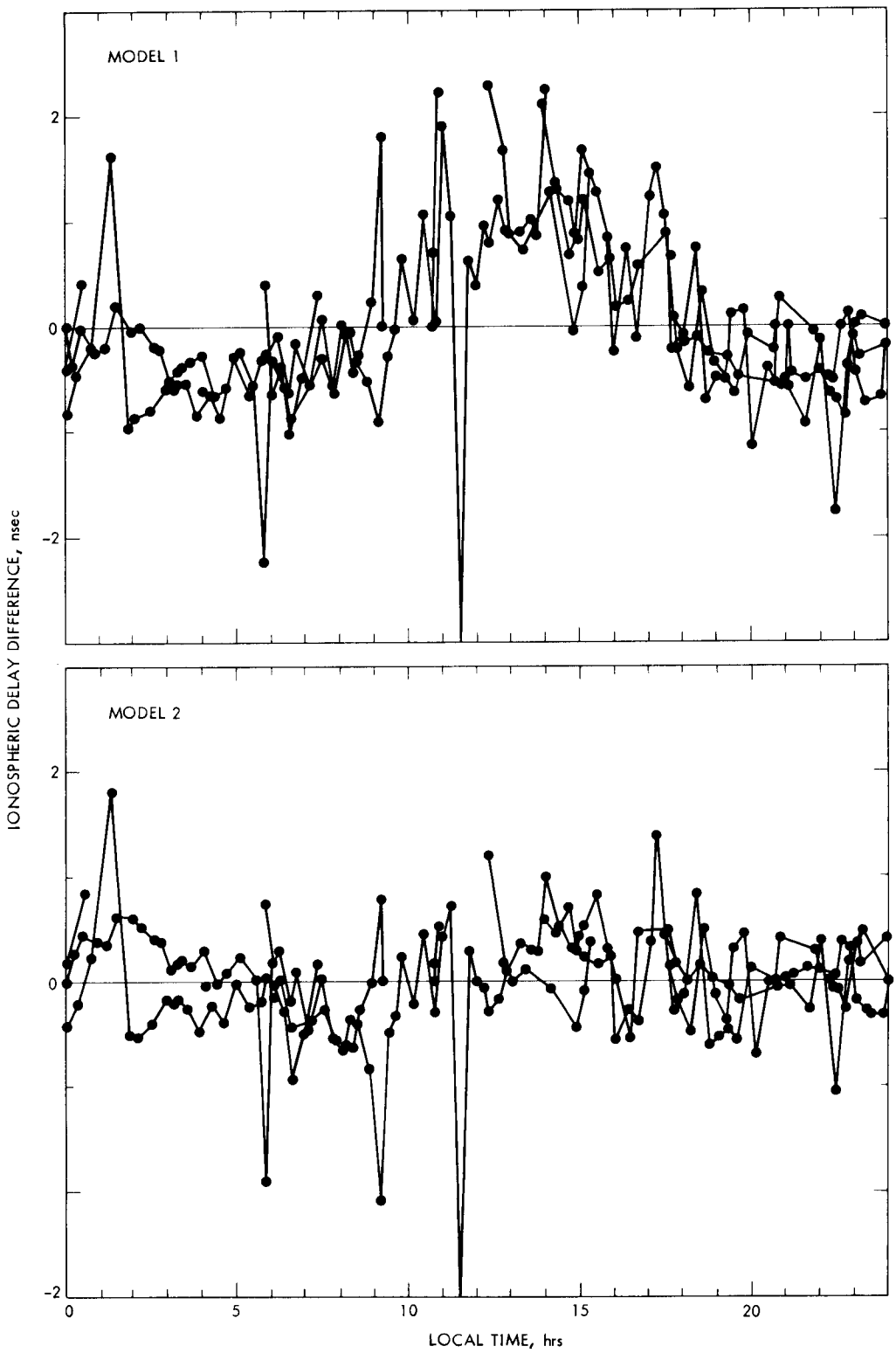

Fig. 7. Dual frequency delay scatter minus Faraday rotation delay scatter versus local time at S-band, experiments 81A, 81B and 81C